JMEPEG
https://doi.org/10.1007/s11665-024-09593-2

©ASM International
1059-9495/$19.00

ORIGINAL RESEARCH ARTICLE

Effect of Pre-strain on Microstructure and Corrosion Behavior of a Novel High-Zn Containing Al-Zn-Mg-Cu Alloy

Mengjun Long, Feng Jiang, Feifei Wu, Mingjin Wu, and Yuanming Su

Submitted: 27 July 2023 / Revised: 14 March 2024 / Accepted: 10 April 2024

The effect of pre-strain on microstructure, mechanical property and corrosion behavior of a novel high-Zn containing Al-Zn-Mg-Cu alloy was investigated by the means of x-ray diffraction, electron back-scattered diffraction, optical profilometer, laser scanning microscope, scanning electron microscope and transmission electron microscopes. The results show that the introduction of pre-strain leads to a decrease in the ultimate strength and elongation of the alloy, which resulting from low density and the larger average size of matrix precipitates. In addition, the ability to resist pitting corrosion, intergranular corrosion and exfoliation corrosion was significantly improved by pre-strain owing to the discontinuous grain boundary precipitates, wider precipitation-free zone and residual dislocations. Among all the pre-strained samples, the 2% pre-strained sample exhibits the best comprehensive performance with optimal corrosion resistance and minimal strength loss; further increasing the degree of pre-stretching, the high-density dislocation and coarsened precipitates within matrix and at grain boundaries accelerated the enrichment of hydrogen at the tip of corrosion crack, resulting in lower corrosion resistance compared with the samples with 2% pre-strain.

Keywords Al-Zn-Mg-Cu alloy, corrosion behavior, microstructure, pre-strain

1. Introduction

Al-Zn-Mg-Cu alloys have been extensively applied in manufacturing aircraft field due to their excellent mechanical properties, fatigue resistance and formability (Ref 1, 2). The attractive combination of properties is attribute to precipitation and grain characteristics formed during heat treatment and artificial aging. In recent years, the breakthrough in ultra-high strength and high corrosion resistance of Al-Zn-Mg-Cu alloy have been a continuous and urgent goal to be achieved. It is believed that optimizing the alloying elements such as increasing the content of Zn element and reducing the Cu element is a feasible approach to achieve the ultra-high strength and excellent corrosion resistance of the new-generation Al-Zn-Mg-Cu alloy (Ref 3-6). As a heat-treatable alloy, the attractive mechanical properties of Al-Zn-Mg-Cu alloy are mainly attributed to the precipitation strengthening mechanism. The generally accepted precipitation sequence for Al-Zn-Mg-Cu alloys can be expressed as: supersaturated solid solution (SSS) $\rightarrow$ GP zones $\rightarrow$ metastable η' phase $\rightarrow$ stable η phase (Ref 7, 8). Numerous researches have indicated that GP zones and metastable η' phase replacing stable η phase are considered to be the fundamental reason for the alloy to reach peak aging (Ref 9-11). In order to obtain excellent mechanical properties, the microstructure and precipitation characteristics of the strengthened phases must be controlled by artificial aging. However, it is hard to maintain a balance between high strength and expected corrosion resistance by the present heat treatment of Al-Zn-Mg-Cu alloys. Generally, the T6 (peaking aging) tempered alloys can achieve obvious strength advantages, but the corrosion resistance and plasticity are weakened. Especially for the ultra-high strength Al-Zn-Mg-Cu alloys with strength above 750 MPa, the industrial applications are remarkably limited due to its poor corrosion resistance (Ref 12). Therefore, it is a great urgency to enhance the corrosion resistance of the alloys while retaining its high strength.

An appropriate pre-strain prior to artificial aging treatment can not only eliminate the residual stress caused by solution quenching, but also modify the precipitation behavior which can be described as dislocations accelerating nucleation and precipitation process during aging heat treatment process (Ref 13, 14). In the past decades, considerable efforts and time have been invested to figure out the impact of pre-stretching on the microstructure and mechanical properties of 7xxx series aluminum alloy. Massive investigates have demonstrated that the pre-strain shows a significant effect on the precipitation behavior of the alloy, and the impacts can be concluded as follows (Ref 15-17). Firstly, dislocations introduced in the matrix by pre-strain provide strong driving force, which promote the nucleation and growth of coarse precipitates. Secondly, dislocations would occupy the positions and alter the concentration of vacancies, resulting in a reduction in the

Mengjun Long, Feifei Wu, and **Yuanming Su**, School of Material Science and Engineering, Central South University, Changsha 410083, China; **Feng Jiang**, School of Material Science and Engineering, Central South University, Changsha 410083, China; and Light Alloy Research Institute, Central South University, Changsha 410083, China; **Mingjin Wu**, Light Alloy Research Institute, Central South University, Changsha 410083, China. Contact e-mail: jfeng2@csu.edu.cn.

Published online: 20 May 2024

diffusion rate of solute atoms, which affecting the precipitation kinetics and the density of precipitated phases. However, controversial conclusions regarding the effects of pre-stretching on the characteristics of GBPs and corrosion resistance of Al-Zn-Mg-Cu alloys have been proposed in various researches. Yuan et al. (Ref 12) reported that the Al-Zn-Mg-Cu alloy attained higher corrosion resistance after pre-strain due to coarse, discontinuous and high copper content GBPs. Moreover, the formation of equilibrium phases with lager size and the reduction in precipitates density show a deleterious consequences among mechanical properties. Han et al. (Ref 18) proposed that compared with the sample without pre-strained, coarse and discontinuous GBPs are more inclined to form in the pre-strained 7075 alloys, with the lower density of precipitates in the matrix. A further investigation by C.R. Shastry (Ref 19) has indicated that the application of pre-strain prior to artificial aging can significantly improve the corrosion resistance of Al-Zn-Mg alloys, which is due to the residual dislocation in the matrix. In addition, pre-strain leads to an evident reduction in the density of heterogeneous precipitation in matrix; without extensive prone corrosion site on the substrate surface, the corrosion resistance of the alloy is significantly ameliorated. However, completely opposite results were obtained in some studies. Lin et al. (Ref 20) have studied the effects of pre-strain on the corrosion behavior of 7475 alloy, the results showed that a rise in the coverage rate of the continuous and coarse GBPs is responsible for the poor corrosion resistance with increasing the pre-strain level. Moreover, same result was indicated by Zhao (Ref 9) and Wang (Ref 21). The research also points out that the application of pre-strain before artificial aging profits for the formation of continuous and fine precipitates at the grain boundaries, which exhibits a detrimental effect on corrosion resistance.

In view of above statements, it is noteworthy that pre-strain before artificial aging treatment has a significant influence on precipitation behaviors and mechanical properties, and it is also hard to ignore that there still exists controversy over the effect of pre-strain on the characteristics of GBPs and corrosion behaviors of Al-Zn-Mg-Cu alloys (Ref 18-24). Therefore, in this paper, the effect of pre-stain on mechanical property and corrosion behavior of a novel high-Zn containing Al-Zn-Mg-Cu alloy is studied. The relationship between pre-strain, precipitation behavior and corrosion behavior have been discussed, which aiming to obtain a more thorough understanding of the role of pre-strain in influencing corrosion behavior of a novel high-Zn containing Al-Zn-Mg-Cu alloys.

2. Materials and Experimental Methods

2.1 Materials Preparation

The materials used in this paper was a novel high-Zn containing Al-Zn-Mg-Cu alloy in the form of 3.3-mm-thick hot-extrusion plate. The main chemical compositions of the studied alloy are shown in Table 1. To obtain the hot-extrusion sheets, the Al-Zn-Mg-Cu alloy ingots with a diameter of 120 mm were prepared by semi-continuous casting, and then the ingots were homogenized at 450 °C/24 h and finally subjected to a hot extruded at 430 °C. The diameter of the ingots used for extrusion were first thinned to 100 mm, and then extruded into plates with a width of 38.3 mm and a thickness of 3.3 mm with an extrusion ratio of 62. The hot-extrusion plates were first subjected to solution treatment at 470 °C for 60 min, followed by rapid water quenching to room temperature. Then, the quenched plates were pre-stretched by 0, 2, 4, 6% along the extrusion direction. Finally, in order to eliminate the effect of natural aging, the plates were aged to T6 temper (120 °C/24 h) immediately after pre-stretching. The specimens for the tensile test were taken parallel to the extrusion direction of the plate. The tensile test was carried out on an RGM-6100 universal testing machine at room temperature with a loading speed of 2 mm/min. For each condition, the tensile properties were obtained by calculating the average values of three samples. The tensile samples were prepared according to the GB/T 228-2002 standard with a gauge length of 50 mm, a width of 8 mm and thickness of 3 mm.

Table 1 Chemical composition of experimental alloy (in wt.%)

Zn	Mg	Cu	Zr	Ti	Fe	Si	Al
9.42	2.84	1.13	0.21	0.05	< 0.02	< 0.01	Bal.

2.2 XRD Analysis

X-ray diffraction (Rigaku SmartLab SE type) was employed to quantitatively calculate the dislocation density of samples with different pre-strain level; the dislocation density can be calculated by the modified Williamson–Hall equation (Ref 25), and the equation is expressed as:

$$\Delta K \cong \frac{\gamma}{D} + \left(\frac{\pi M^2 b^2}{2}\right)^2 \rho^{\frac{1}{2}} K\overline{C}^{\frac{1}{2}} + \mathrm{O}(K^2\overline{C}) \quad \text{(Eq 1)}$$

where ΔK also equals to $(\beta\cos\theta)/\lambda$, β is the full width at half maxima (FWHM) obtained by diffraction of peak XRD patterns, λ equals to 0.154046 nm, θ is diffraction angle and γ equals 0.9. D is the coherently scattering domain size, and b and ρ represent the absolute value of Burgers vector of dislocation (b = 0.286 nm in aluminum alloy) and dislocation density, respectively. M represents the dislocation arrangement parameter (M values 1-2 in deformed alloy) (Ref 26, 27). K equals to $(2\sin\theta)/\lambda$, which represents modulus of the diffraction vector. $\mathrm{O}(K^2\overline{C})$ represents the higher order term residue. $\overline{C}$ is the contrast factor of dislocations, which depends on the orientation relationship between the Berger vector, diffraction vector, line vector of dislocations and elastic constants of the materials (Ref 27). For cubic crystal materials, the contrast parameter can be obtained by the fourth-order polynomial of Miller's indices (Ref 25, 27):

$$\overline{C} = \overline{C}_{h00}(1 - qH^2) \quad \text{(Eq 2)}$$

where $\overline{C}_{h00}$ is the average contrast factor of $h00$ reflections, q depends on the ratios of edge and screw dislocation and the elastic constants of the materials; the H value can be obtained from the diffraction index of the material (Ref 28):

$$H^2 = (h^2k^2 + k^2l^2 + h^2l^2)/(h^2 + k^2 + l^2) \quad \text{(Eq 3)}$$

From Eq 1, 2 and 3, the dislocation density can be obtained by the slope of the plot of ΔK as a function of $K\overline{C}^{\frac{1}{2}}$.

2.3 Corrosion Evaluation

The corrosion behavior was investigated by immersion corrosion test, intergranular corrosion (IGC) test and exfoliation corrosion (EXCO) experiment. In order to ensure the credibility and repeatability, three parallel samples were prepared in each corrosion test. Before corrosion tests, all samples were grinded and mechanical polished to exclude the influence of other unrelated factors. Immersion tests were carried out in 3.5% NaCl solution (wt.%) for 48 h, and the temperature of the solution was maintained at 25 ± 1 °C as described in the standard of ASTM corrosion tests (Ref 29). After the samples were etched, the corrosion morphologies and the depths of corrosion pits of the samples were captured with polarizing microscopy (LEICA DMILED DFC295 type) and optical profilometer (Wyko NT9100 type), respectively. For IGC tests, according to the GB/T 7998-2005 standard (Ref 30), the samples were bathed in the deionized-water electrolyte solution of 57 g/L NaCl + 10 mL/L H_2O_2 at 35 ± 1 °C. After continuous immersing for 6 h, the IGC morphologies and depths were obtained by using scanning electron microscope (SEM, JEOL, JSM-IT200 type) equipped with energy dispersive spectroscopy (EDS). The EXCO tests were carried out according to the standard of ASTM G34 (Ref 31, 32). The solution contains 4 M NaCl + 0.5 M KNO_3 + 0.1 M HNO_3. The immersion time is 48 h, and the solution temperature is maintained at 25 ± 1 °C. The three-dimensional EXCO surface topographies of the samples were observed by laser scanning confocal microscopy (Zeiss Axio LSM700 type).

2.4 Microstructural Characterization

The grain microstructures of the samples after pre-strain were observed by filed-emission scanning electron microscope (JEOL, JSM-7900F type) equipped with electron backscatter diffraction (EBSD) detector, scanning with a step size of 0.2 μm and a voltage of 20 KV. The data collected by EBSD were analyzed by Channel 5 software.

The residual dislocation distribution, grain microstructures and precipitation characteristics within matrix and grain boundaries after aging treatment were observed by transmission electron microscope (TEM). The samples used for TEM observation were polished and mechanically thinned to a thickness with 60-80 μm, and then the samples were electropolished and perforated by an MTP-1 Twin-jet electropolishing machine. The electrolyte was a mixed solution of 30% nitric acid and 70% methanol, and the electrolytic temperature was maintained at − 30 to − 20 °C. Afterward, the TEM samples were observed at an electron microscope (FEI Tecnai G2 F20 type) with an operating voltage of 200 kV.

3. Results

3.1 Microstructure Characterizations and Mechanical Properties of Studied Al-Zn-Mg-Cu Alloy

Figure 1(a) shows the XRD patterns of Al-Zn-Mg-Cu alloy plates with various pre-strained degree; hence, the FWHM of the pre-strained samples can be obtained. According to Eq 1, 2, and 3, the liner fittings of ΔK as a function of $K\overline{C^2}$ are shown in Fig. 1(b). In order to calculate the value of dislocation density, the slopes of the liner fitting are indispensable, and the slopes values of 0-6% pre-strained samples can be calculated, which are 0.67×10^{-4}, 0.57×10^{-3}, 0.71×10^{-3} and 0.96×10^{-3}, respectively. From the slopes, the dislocation density of the samples with 0, 2, 4 and 6% pre-strained can be calculated as $3.54 \times 10^{12}/m^2$, $2.49 \times 10^{14}/m^2$, $3.93 \times 10^{14}/m^2$ and $7.16 \times 10^{14}/m^2$, respectively. It is obviously that pre-strain shows a significantly influence on the dislocation density in the alloy matrix. For the samples without pre-strained, the dislocation density is pretty low. When the alloy sheets are applied to various pre-strain level, the dislocation density in the alloy accumulates and increases rapidly as the degree of pre-stretching increases from 0 to 6%.

The microstructure characterization of the samples after pre-strain and before aging is shown in Fig. 2. After solution heat treatment, as shown in Fig. 2(a_1), the grains of un-strained samples are typical equiaxed crystal structure. The most intuitive impact on microstructure caused by pre-strain is the change of grain morphology, and the grains were stretched along the pre-straining direction and presented as fibrous crystal. The inverse pole figures (IPF) of samples with different pre-strain levels are shown in Fig. 2(a_2) and (d_2). The white lines and red lines indicate the location of low-angle grain boundaries (LAGBs) with misorientation between 2° and 15° and the high-angle grain boundaries (HAGBs) with misorientation greater than 15°, respectively. It can be seen that with the level of pre-strain increasing from 0 to 6%, the proportion of LAGBs increased from 23.5 to 46.7% (Fig. 2a_4 and d_4). Correspondingly, the values of kernel average misorientation (KAM) increased gradually as the increasing pre-strain level (Fig. 2a_5 and d_5); a higher KAM value indicates a greater degree plastic deformation or a higher geometrically necessary dislocation (GND), which is consistent with the results of GND maps obtained in Fig. 2(a_3) and (d_3).

Table 2 shows the tensile mechanical properties of the Al-Zn-Mg-Cu alloy plates applied different pre-strain level. Obviously, pre-strain shows a negative effect on mechanical properties of the alloy. Among all the samples, it can be seen that the ultimate strength (UTS) and elongation of pre-strained sample were all lower than unstretched samples. As the pre-strained level increased from 0 to 6%, the UTS and elongation of the Al-Zn-Mg-Cu alloy decrease from 742.1 MPa and 6.9% to 699.7 MPa and 6.2%, respectively, whereas the yield strength (YS) first increases and then decreases. The corresponding fracture morphology is shown in Fig. 3. As shown in Fig. 3(a) and (b), dimples with various sizes can be obviously observed in the unstretched samples. After 2% pre-strained treatment, the dimples with smaller size and lesser quantity can be observed on the fracture surface (Fig. 3d). When the induced pre-strain increased to 4%, the number of dimples decreases dramatically, tearing ridges and smooth fracture surface appeared between grain boundaries (Fig. 3e and f). As for the 6% pre-strained samples, the marks of fracture edges become more conspicuous and sharper, and large regions of smooth sliding surface appeared, which are responsible for the lower elongation.

3.2 Corrosion Behavior

Figure 4 shows the surface corrosion morphologies of the aged samples with different pre-strained after immersion in 3.5% NaCl solution for 48 h. As seen in Fig. 4(a) and (d), all samples exhibit evident corrosion pits, but the corrosion surface of the samples with different pre-strains presented remarkable

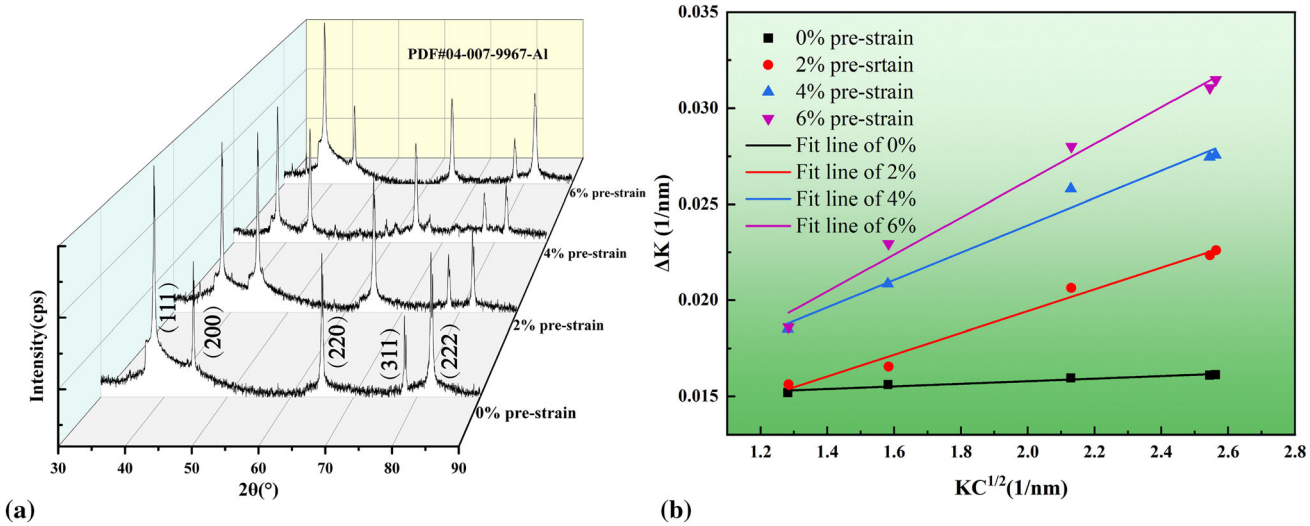

Fig. 1 Dislocation density analysis by XRD. (a) XRD patterns of different samples; (b) Liner fitting of ΔK and $K\overline{C^2}$

differences. After pre-strained, the number of corrosion pit on the alloy surface is significantly reduced and distributes more scattered compared with un-strained samples. For un-strained alloy plates, thickly dotted corrosion pits are continuous along the extrusion direction after soaking in 3.5% NaCl solution for 48 h (Fig. 4a). As for the 2% pre-strained samples, the density of pitting pits reduced remarkable and scattered distribution on surface, which indicates a significant improvement in corrosion resistance (Fig. 4b). Moreover, it is worth noting that as the pre-strain level increase to 4% and 6%, especially for 6% pre-strained plates, the number of pitting pits on the alloy surface increases noticeably and becomes continuously distributed (Fig. 4d). The maximum depths of corrosion pits corresponding to Fig. 4 are shown in Fig. 5. In the present work, the uncorroded areas above adjacent corrosion pits on the alloy surface are considered as the reference horizontal line, so the depths of the corrosion pits in different samples can be taken as the distance between the lowest point in the pit and the reference plane. The maximum depths of the samples pre-strained 0-6% are 45.13, 12.43, 15.14 and 18.22 μm, respectively. Comparatively, the samples with 2% pre-strain application exhibits more excellent corrosion resistance, which is consistent with the results shown in Fig. 4. The above results are taken as supports that a suitable pre-strain does appear to improve the corrosion resistance of studied Al-Zn-Mg-Cu alloy.

The intergranular corrosion depth and typical IGC morphologies of the alloys with various pre-strain levels after IGC test are shown in Fig. 6. According to the IGC morphology, the depth of intergranular corrosion is significantly reduced after pre-strained treatment, which indicates a better intergranular corrosion resistance of pre-strained samples. It can be seen that the samples without pre-strained were most sensitive to IGC, of which exhibited the deepest depth of intergranular corrosion (79.53 μm), and the surface layer of the alloy was sever peeled off and corroded, as shown in Fig. 6(a). After exerting 2% pre-stretching, the corrosion resistance of the Al-Zn-Mg-Cu alloy shows a significant improvement and has the lowest IGC depth of about 40.11 μm (Fig. 6b). When continued to increase in the pre-strain, the IGC depths of 4 and 6% pre-stretched plates are 57.42 and 60.23 μm, respectively. Compared to the samples with 2% pre-strained, the improvement in intergranular corrosion resistance is limited in high pre-strained samples. In addition, compared with un-strained samples, application of 2% pre-strain can also greatly reduce the width of IGC cracks. In un-strained samples, intact grains are severely corroded along the grain boundaries and corrosion penetrated into the interior of the alloy, leading to extensive corrosion products of $Al(OH)_3$ and exfoliation products (Fig. 6e_1 and e_4). As for 2% pre-strained samples, only local corroded regions were observed on the surface of the sample, and the corrosion products mainly exist along the corrosion cracks with few intact grains are corroded completely (Fig. 6f_1 and f_4).

Compared to immersion and IGC tests, the EXCO tests can intuitively reflect the ability of intergranular corrosion resistance under worse corrosion environment. Figure 7 shows the 3D surface topography of the samples after EXCO tests. For the un-strained sample, a large scale of peeling off in flakes occurs on the surface, numerous deep corrosion pits with around 250-300 μm are visible, and adjacent corrosion pits are connected to penetrate the alloy surface (Fig. 7a). After applying various degrees of pre-strains, the unevenness of the surface and scattered corrosion pits indicates that the exfoliation corrosion resistance has been improved in differ degree. Comparatively, subjection of 2% pre-strain can significantly reduce the width and depth of exfoliation corrosion pits, of which with a maximum depth of approximately 100-120 μm. With the pre-strain level increases to 4% and 6%, the area peeled off on the surface becomes wider, and the depth of corrosion pits is deeper. Therefore, it is reasonable to conclude that pre-strain (especially 2% pre-strain) does enhance the ability of exfoliation corrosion resistance of the experimental alloys, which is consistent the results of IGC tests shown in Fig. 6.

3.3 Precipitation Behavior

Figure 8 shows the dislocations, typical GBPs and matrix precipitates (MPts) of the experimental Al-Zn-Mg-Cu alloy plates applied to 0-6% pre-strain. As shown in Fig. 8(a_1), (d_1), (a_2), and (d_2), when compared to the samples subjected to 0-6% pre-strain before aging, although the dislocation induced by pre-strain has been effectively eliminated after aging heat treatment among all the samples, varying degrees of dislocation structure still can be observed in pre-strained samples (Fig. 8b_2

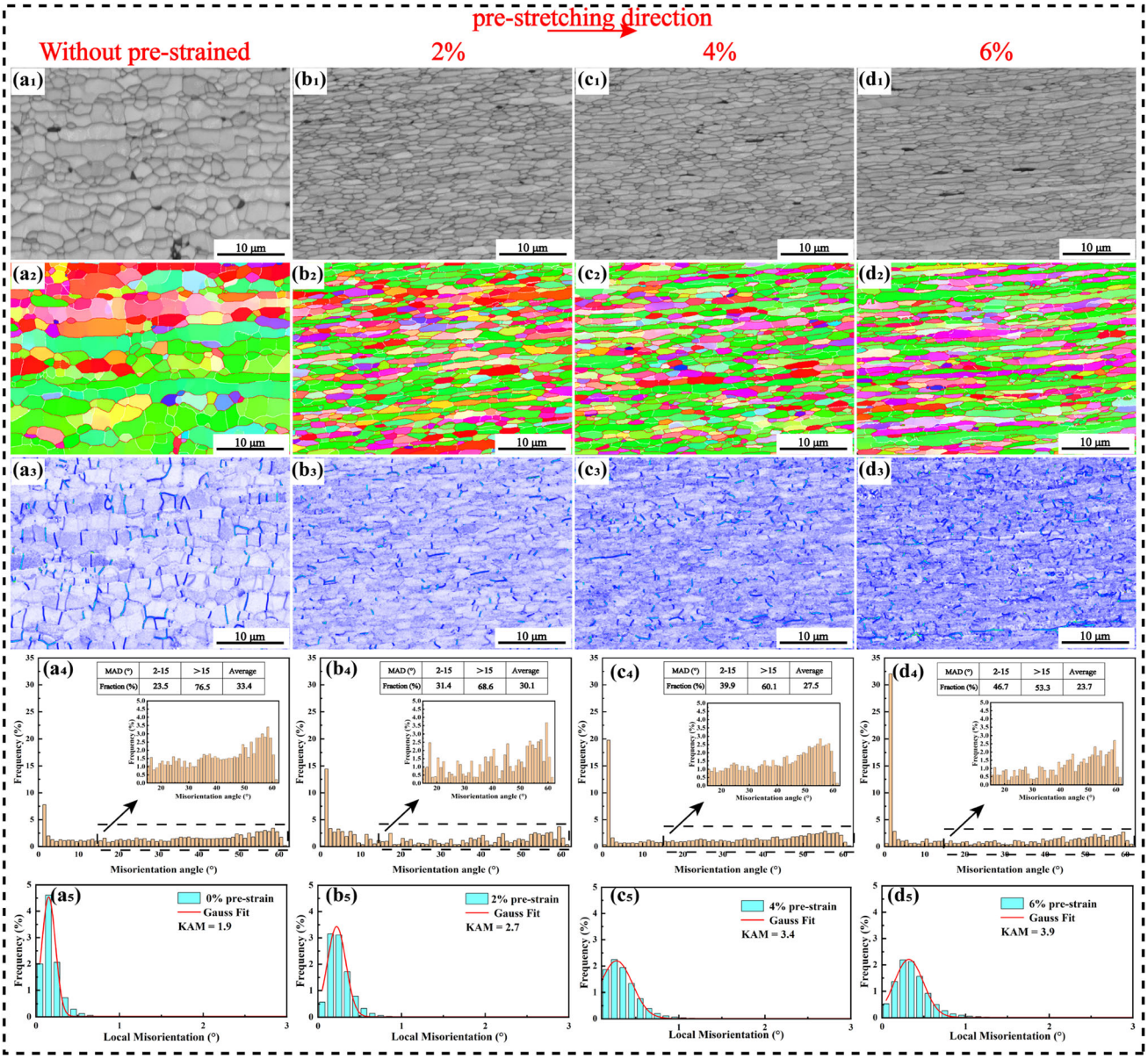

Fig. 2 Microstructure, IPF diagrams, GND graphs, misorientation angle distribution and KAM distribution of studied alloys. (a_1–a_5) without strain; (b_1–b_5) 2% pre-strain; (c_1–c_5) 4% pre-strain; (d_1–d_5) 6% pre-strain

Table 2 Mechanical properties of experimental alloy various with different conditions

Samples	UTS, MPa	YS, MPa	Elongation, %
0% + T6	742.1 ± 6.0	687.2 ± 5.0	6.9 ± 0.3
2% + T6	727.4 ± 4.0	695.6 ± 3.0	6.7 ± 0.2
4% + T6	719.3 ± 3.0	683.4 ± 3.0	6.4 ± 0.3
6% + T6	699.7 ± 5.0	663.6 ± 4.0	6.2 ± 0.3

and d_2). In addition, compared with typical recrystallized equiaxed grain in un-strained samples, the proportion of sub-structures increases with increasing pre-strain level. Through comparing the characteristics of GBPs and MPts in different samples, pre-strain does generate a remarkable influence on the precipitation behavior. In the un-strained samples, a high-density of fine precipitates homogeneously distributed within the matrix, and a mass of GBPs continuously along the grain boundary can be observed (Fig. 8a_3 and a_4). For the pre-strained alloy plates, the characteristics of GBPs changed apparently, as shown in Fig. 8(b_3) and (d_3). In 2% pre-strained samples (Fig. 8b_3), discontinuously coarsened η precipitates can be clearly observed at the grain boundary, with a lower density of GBPs and wider PFZ. As the pre-strain increased to 4% and 6%, the GBPs coarsen to larger sizes, and the spacing between adjacent GBPs becomes narrower. Notably, among all pre-strained samples, the coarsened η particles show obvious orientation characteristics and preferably precipitate and coarsen on grain boundary (Fig. 8b_3 and d_3), which illustrates that the dislocation introduced by pre-strain promotes the nucleation and coarsening of η particles during aging. Furthermore, the MPts morphologies of different samples are shown in Fig. 8(a_4) and (d_4). Compared to the samples without pre-

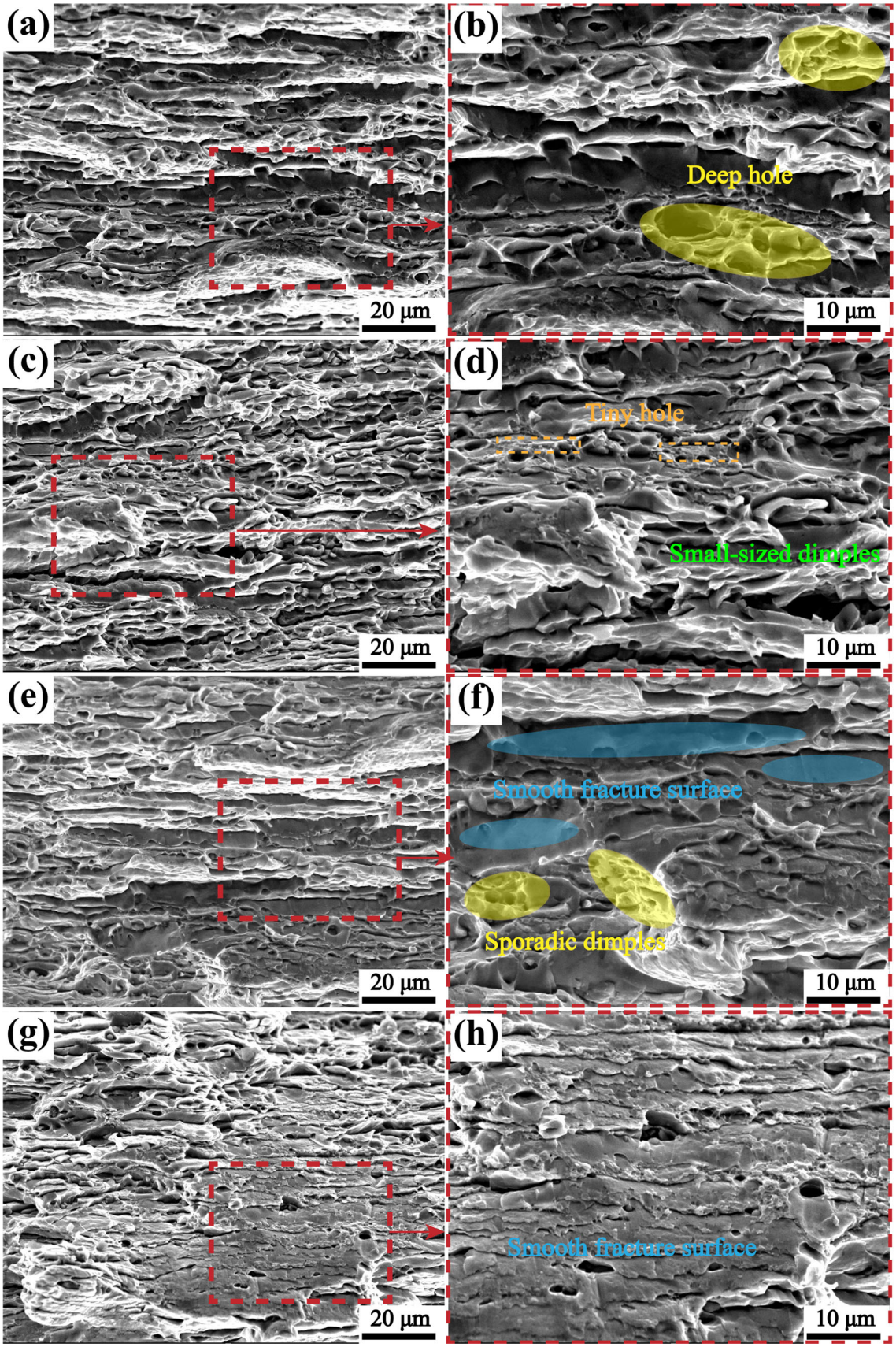

Fig. 3 Fracture morphologies of the alloy under various aging stages: (a, b) 0% + T6; (c, d) 2% + T6; (e, f) 4% + T6; (g, h) 6% + T6

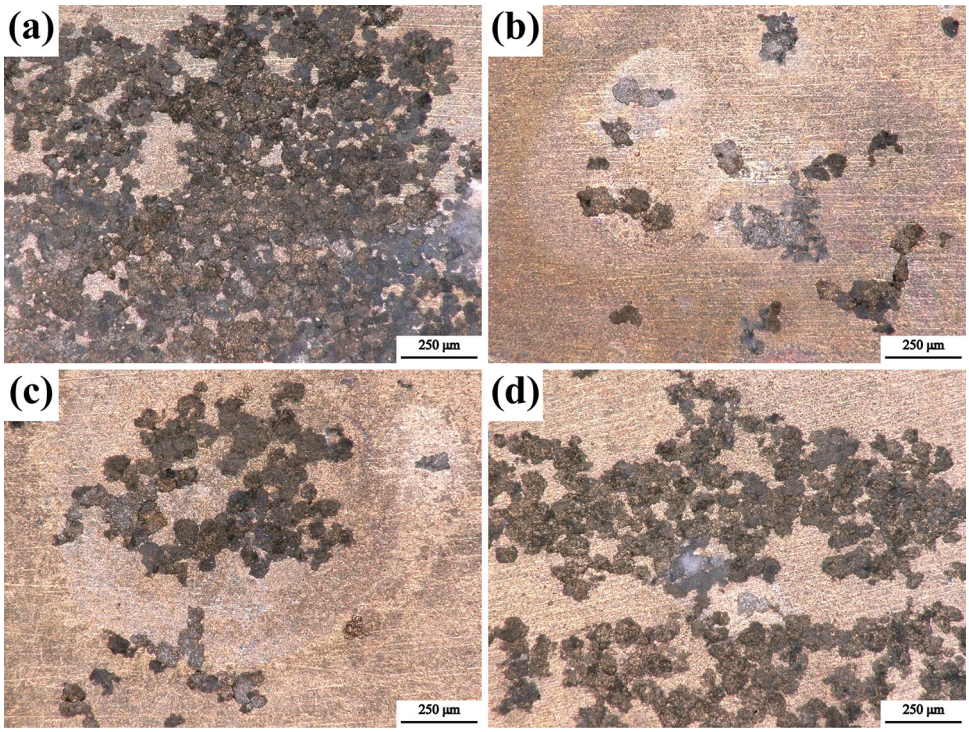

Fig. 4 Surface corrosion morphologies after immersion in 3.5% NaCl solution for 48 hours: (a) 0% + T6; (b) 2% + T6; (c) 4% + T6; (d) 6% + T6

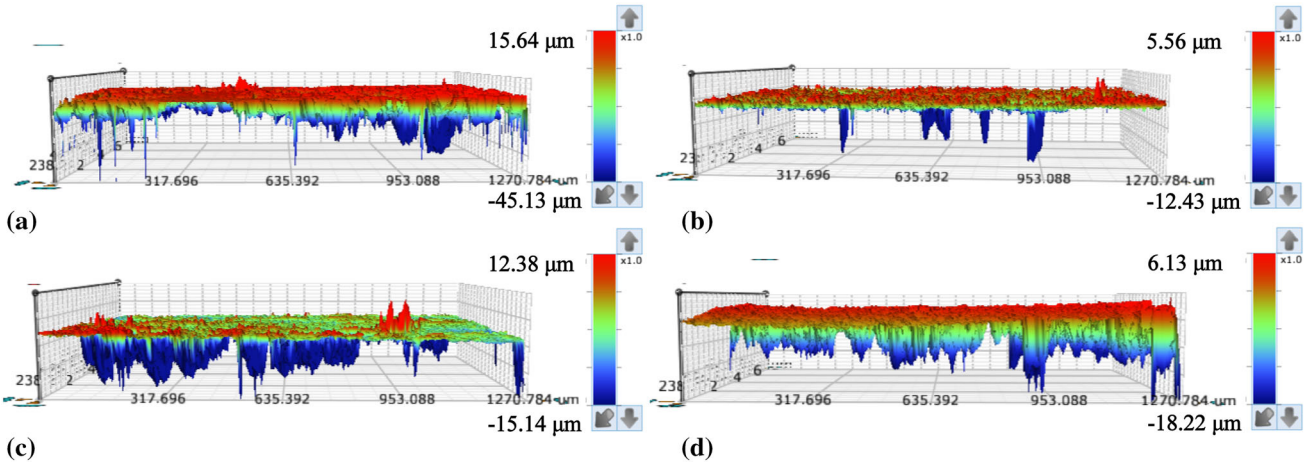

Fig. 5 Maximum depth of corrosion pits after immersion in 3.5% NaCl solution for 48 h: (a) 0% + T6; (b) 2% + T6; (c) 4% + T6; (d) 6% + T6

stretching, the size of MPts was lager, and the average diameter increased from 4.14 to 4.92 nm (Fig. 8a_5 and d_5); the corresponding is a relatively low density of MPts presented in pre-strained samples.

4. Discussion

4.1 Effect of Pre-strain on Microstructure and Mechanical Properties of Al-Zn-Mg-Cu Alloy

The intuitive influence of pre-strain prior to aging on microstructure is the proliferation of dislocation in Al-Zn-Mg-Cu alloy, and the TEM micrograph shown in Fig. 8(a_1) and (d_1) exhibits an obvious characteristic that the dislocation induced by pre-strain distribute uniformly in the form of dense tangled forest. The results analyzed in Fig. 1 quantitatively demonstrate a liner increase in dislocation density with the increase in pre-strain degree, which are consistent with the results shown in Fig. 8. Extensive researches have reported that the defects such as dislocation show significant effect on the precipitation and performance of alloy (Ref 13, 33). In the present work, applying plastic deformation (even 2% pre-strain samples) before aging introduce a large number of dislocation and vacancies. As for Al-Zn-Mg-Cu alloy, the generally accepted precipitation sequence can be expressed as: supersaturated solid

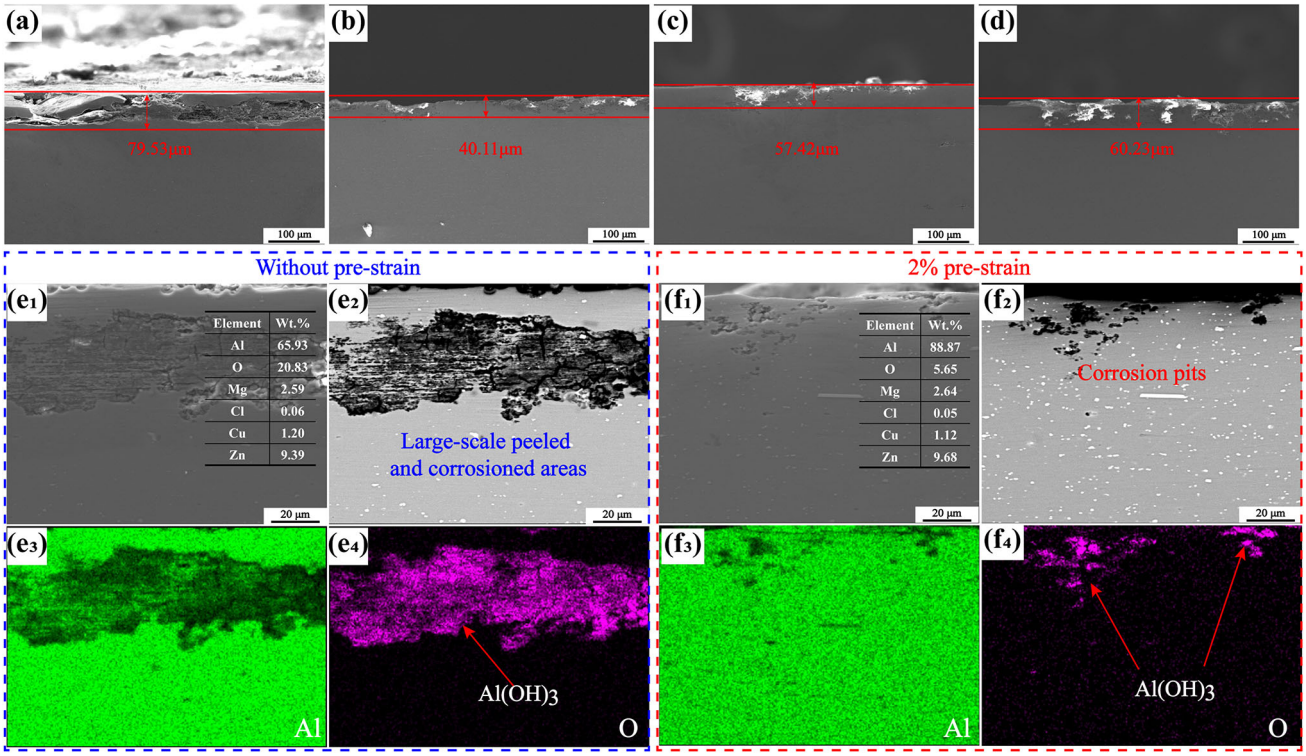

Fig. 6 IGC morphology and maximum depth of studied alloys. (a) 0% + T6; (b) 2% + T6; (c) 4% + T6; (d) 6% + T6; (e), (f) EDS analysis of 0% + T6 and 2% + T6 samples, respectively.

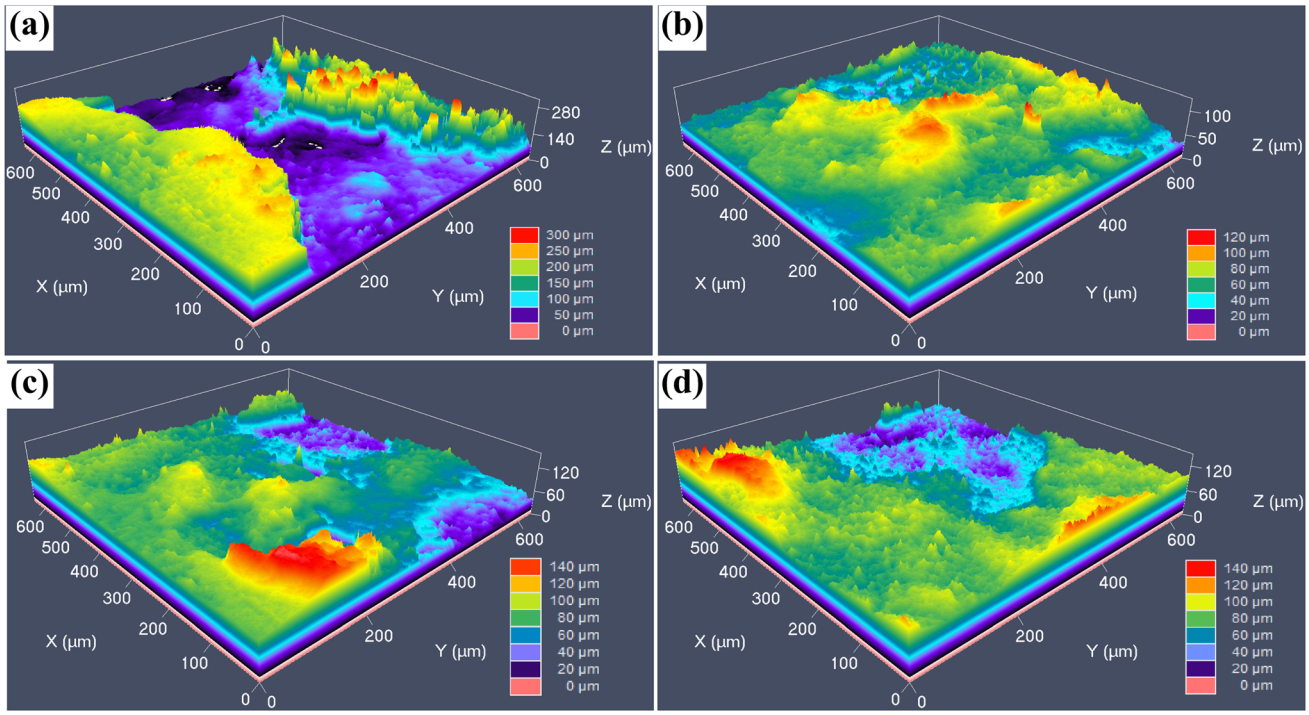

Fig. 7 Three-dimensional surface topography of the Al-Zn-Mg-Cu alloys after EXCO tests: (a) 0% + T6; (b) 2% + T6; (c) 4% + T6; (d) 6% + T6

solution (SSS) → GP zones → η' phase → η phase. The uniformly distributed dislocation provided sufficient driving force for the nucleation and growth of η'/η phase and promoted the transition process of η' phase → η phase. On the one hand, in the early aging stage, extensive coarsened phases preferentially form at the regions with high dislocation density (especially at the grain boundary), which resulting discontinuous and coarse GBPs in the pre-strained samples (Fig. 8b_3 and

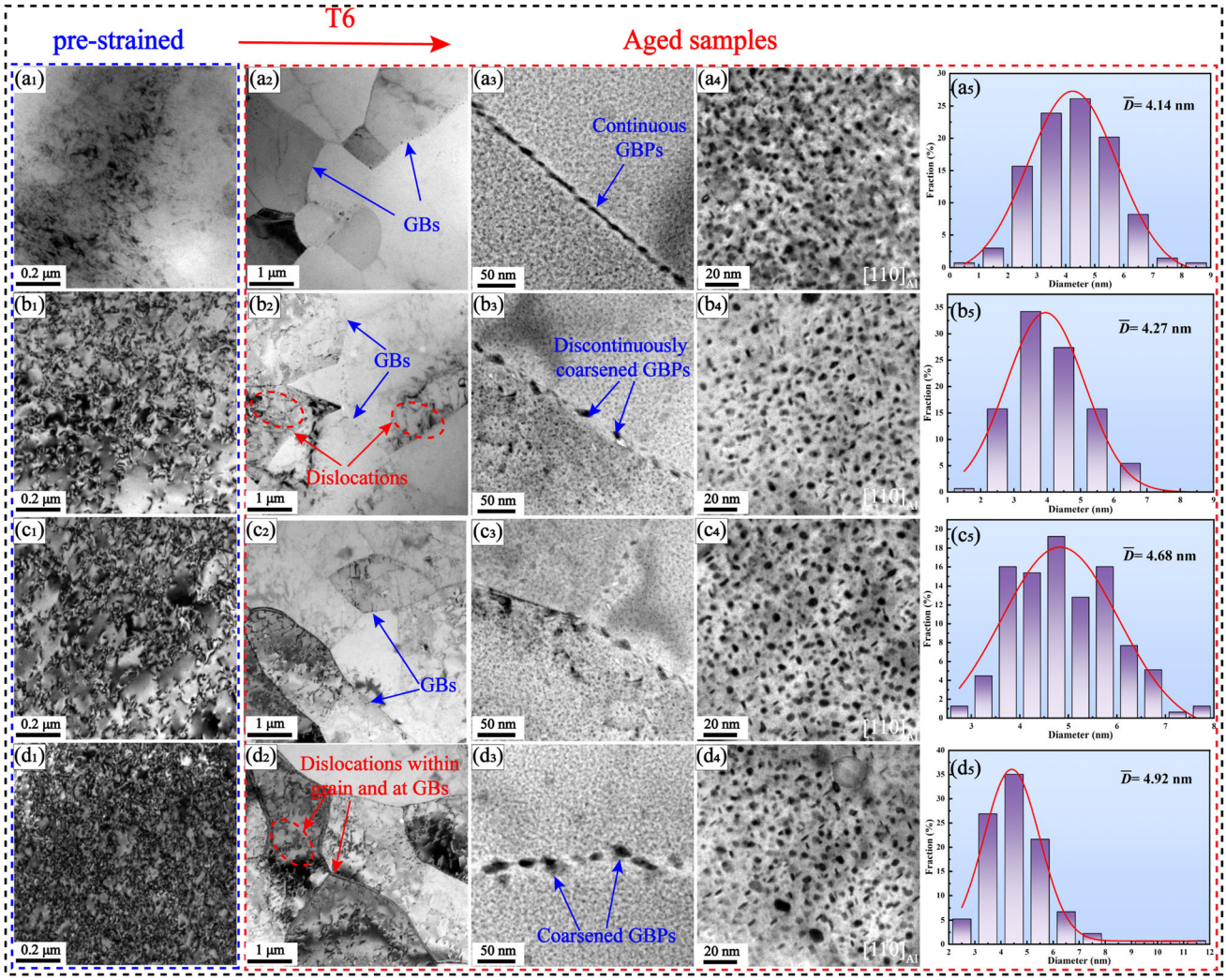

Fig. 8 TEM images of the samples subjected to different pre-strain level and the diameter distribution of the MPts. (a_1–a_4) 0% + T6; (b_1–b_4) 2% + T6; (c_1–c_4) 4% + T6; (d_1–d_4) 6% + T6

d_3). Besides, the rapid reduction in vacancy density during pre-stretching decreases the nucleation sites for GP zone and η' phase, and the preferentially nucleated η phase consumed solute atoms. On the other hand, the dislocation serves as a fast diffusion path for solute atoms due to the low diffusion activation energy, which accelerate the coarsening of the precipitates (Ref 16, 34). Figure 9 shows the morphology of dislocation and MPts in 0%, 2% and 6% pre-strained alloy plates. It can be seen that with the increase in pre-strain level, the size of precipitates increases visibly. The coarser and rode-shaped precipitates were heterogeneously distributed in the 6% pre-strained samples while compared with un-strained and 2% pre-strained samples, which indicates that the high-density dislocation remarkably promoted aging precipitation process (Fig. 9a_2 and c_2). Correspondingly, the high-resolution transmission electron microscopy (HRTEM) images are presented in Fig. 9(a_3) and (c_3). In the un-strained samples, a large number of fine dispersed η' phases and GP zones can be observed inside the grains (Fig. 9a_2 and a_3), which are considered as the reason for the highest strength of the alloy. After application of pre-strain, the precipitates are coarsened, and rode-shaped precipitate with larger diameter identified as semi-coherent η' phase can be found in the 2% pre-strained samples (Fig. 9b_3), while coarse precipitate considered as incoherent η phase can be observed in 6% pre-strain samples (Fig. 9c_3). In addition, as the aging temperature is considerably lower than recrystallization temperature, majority of dislocation annihilated each other and the rest exist in the form of substructure such as dislocation walls after aging, which are consistent with the results shown in Fig. 9(a_1) and (c_1). Thus, from the above observations, it is logical to conclude that pre-strain exhibits a significant impact on the precipitation behavior of Al-Zn-Mg-Cu alloy, and lower density of MPts and coarser precipitates is observed in the pre-strained alloys, which results in the strength reduction in the alloy.

4.2 Effect of Pre-strain on Corrosion Behavior of Al-Zn-Mg-Cu Alloy

Pitting corrosion is regarded as the most typical corrosion type of the Al-Zn-Mg-Cu alloy in the chloride-containing solution, which could occur at Al matrix, insoluble phases such as Al_2CuMg and Al_7Cu_2Fe phases (Ref 29, 35). In the present study, pitting corrosion at Al matrix is attributed to the dispersed strengthening phase such as GP Zones, η' and η phases. Preferential pitting corrosion could occur at these MPts

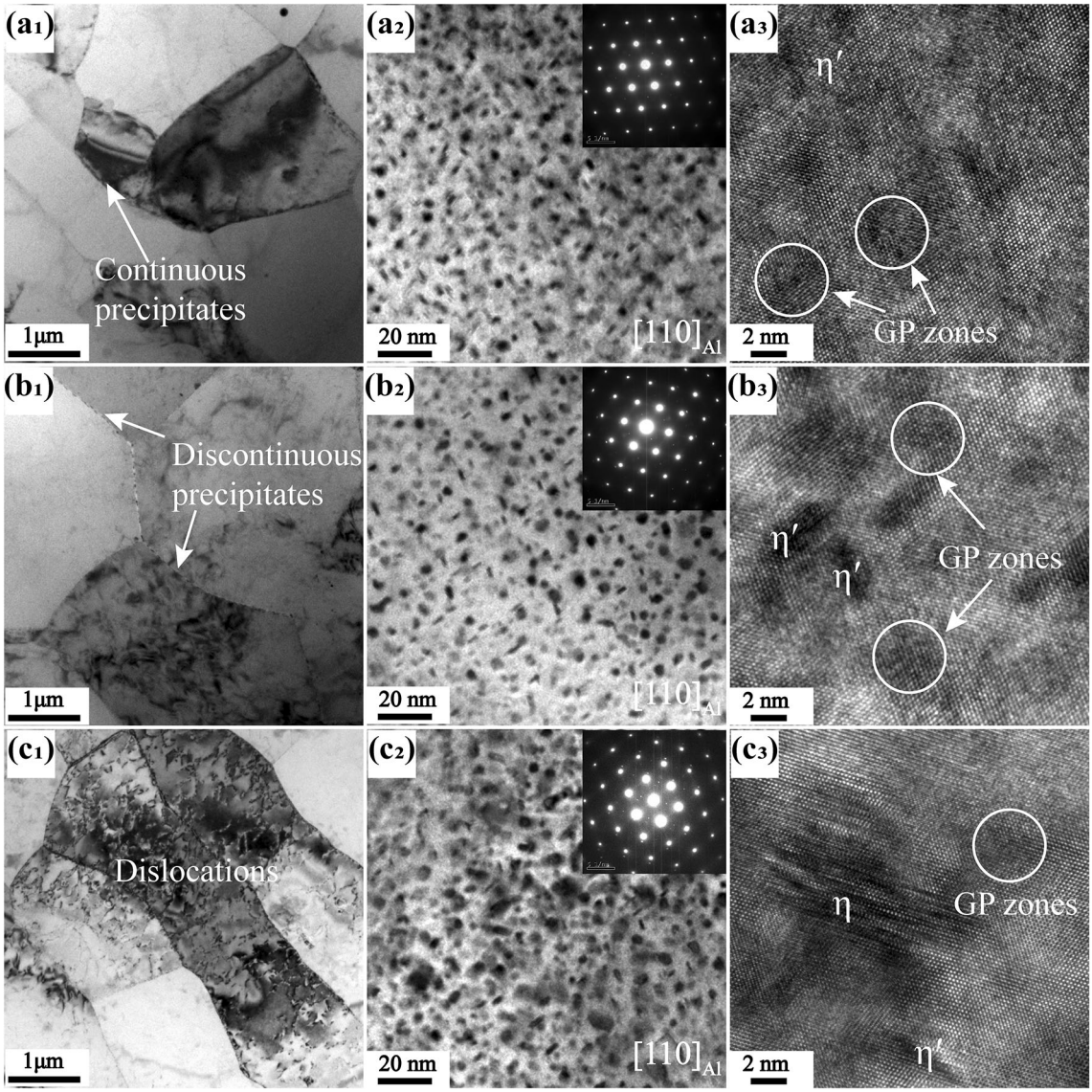

Fig. 9 TEM images of dislocation, MPts and HRTEM images: (a_1–a_3) 0% + T6; (b_1–b_3) 2% + T6; (c_1–c_3) 6% + T6

enriched with Zn and Mg atoms due to the lower potential than that of Al matrix, which leads to the formation of corrosion pits (Ref 36-39). As shown in Fig. 8 and 9, the densely distributed second phases in un-strained samples provide extensive potential sites for the pitting corrosion of the Al-Zn-Mg-Cu alloys, resulting in large-area continuous pitting corrosion in the immersion test (Fig. 4a). In the 2% pre-strained plates, the number of the corrosion pits on the alloy surface are significantly reduced due to the lower density of MPts. However, limited improvement on corrosion resistance is displayed in high pre-deformation samples (Fig. 4c and d), that is because except for the density of MPts, the coarse precipitates within matrix are also considered as an adverse factor for anti-corrosion (Ref 40, 41). As shown in Fig. 9(c_2), extensive coarsened η' phases and η phases can be observed in 6% pre-strained samples, which weakening the corrosion resistance as the coarsened precipitates act as the anode and be attacked preferentially. Besides the improvement of the ability to resist pitting corrosion, the ability to resist intergranular corrosion can also be reinforced by pre-strain. Previous investigations have reported that the intergranular corrosion resistance of Al-Zn-Mg-Cu alloy is closely related to the characteristics of GBPs (Ref 20, 35). The GBPs morphology shown in Fig. 8(a_3) presents concentrated and continuously distributed precipitate along the grain boundary in the un-strained samples. Hence, during the corrosion process, a preferential anodic channel is easily formed along the grain boundary, which significantly promote the corrosion rate of the Al-Zn-Mg-Cu alloy. Because the grain boundary is preferentially corroded, the binding force of adjacent grain decreases dramatically, which results in delamination corrosion between layers in IGC experiment (Fig. 6a) and severe peeling corrosion in EXCO tests (Fig. 7a). Figure 10 shows the distribution of MPts, corrosion morphology and EDS analysis of without pre-strained and 2% pre-strained samples. The results shown in Fig. 10 are consistent with the above conclusions; as for the un-strained samples, the continuous MPts are responsible for the poor corrosion resistance of the samples. The alloy surface was severely peeled off, a large amount of residual corrosion products can be observed, and the grains were completely

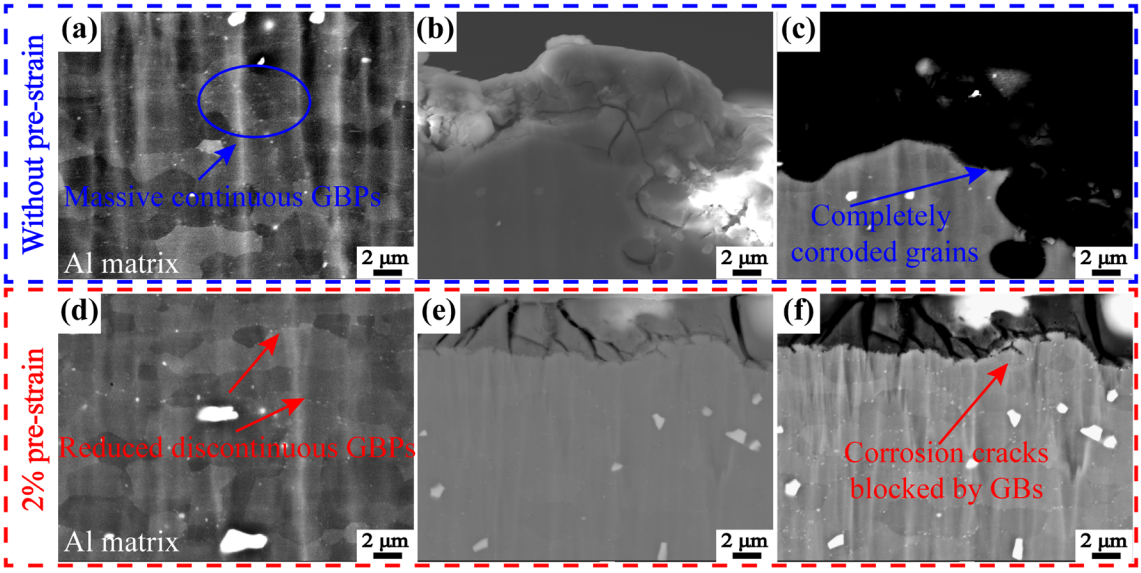

Fig. 10 Distribution of MPts, corrosion morphology and EDS analysis of different samples: (a–c) without pre-strain; (d–f) 2% pre-strain

corroded (Fig. 10b and c). In the present work, the higher corrosion resistance of pre-strained samples was attributed to discontinuous GBPs and wider PFZ. In the pre-strain samples, the discontinuous and widely spaced GBPs effectively prevent the persistent occurrence of corrosion along the grain boundaries (Fig. 10e and f). From the results mentioned above, it can be concluded that an appropriate pre-strain (2%) has a significant improvement on the corrosion resistance, but excessive pre-strain stimulates the formation of coarse GBPs and η phases within matrix, which manifesting negative impact on corrosion resistance.

In addition, it is believed that the residual dislocation after aging treatment play an important role in susceptibility to corrosion of Al-Zn-Mg-Cu alloy (Ref 42). The TEM images shown in Fig. 8 and 9 indicate that there are still residual dislocations in the samples with various pre-strain after artificial aging treatment; hence, the effect of residual dislocation on corrosion should be taken into account. In general, the dislocation serves as a rapid diffusion path for hydrogen ions, which promotes the concentration of hydrogen at the tip of corrosion crack, thus accelerating the corrosion process. The coarse phase and high-density residual dislocation are responsible for its worse corrosion resistance in 6% pre-strained samples (Fig. 9c_1). However, compared with the samples without pre-strained and high pre-strained, 2% pre-strained samples show the better comprehensive properties. In the present work, based on the combination of above investigation and analysis, a more reliable conclusion is obtained to reveal the synergistic of residual dislocations, GBPs and MPts on the corrosion resistance of the high-Zn containing Al-Zn-Mg-Cu alloy. For the samples without pre-strain, the grain boundaries are preferentially corroded due to continuous GBPs, and an acidification environment is easily formed at the crake tip as massive corrosion products accumulate in the corrosion crack gap. The accumulation of hydrogen provides favorable conditions for corrosion and promote the expansion of crake along the grain boundary. Compared with un-strained samples, the evident improvement on corrosion resistance in 2% pre-strained samples are attributed to following factors. Firstly, the introduction of dislocation leads to coarse and discontinuous GBPs, which effectively prevent the crack propagation. Secondly, it was demonstrated that dislocation form a fast diffusion channel for Cu atoms toward grain boundary, thus weakening the corrosion dynamics due to the lower potential difference between GBPs and matrix (Ref 12). Thirdly, as shown in Fig. 8(b2) and 9(b1), tiny amounts of dislocations still can be observed in the 2% pre-strained samples after aging heat treatment. These dislocation wall and sub-structures serve as traps for hydrogen atoms, and the hydrogen atoms were captured by dislocations or coarse η phases, which limits the diffusion of hydrogen to the grain boundary and crack tip (Ref 12, 43). Additionally, with the pre-strain increase to 4 and 6%, the high-density residual dislocation accelerates the breakdown of the passivation film and increases the hydrogen embrittlement susceptibility of the studied alloy, which is the reason for poorer corrosion resistance in high pre-strained samples. As a result, a 2% pre-strain exhibits a significant improvement on corrosion resistance of Al-Zn-Mg-Cu alloy.

5. Conclusions

1. The introduction of pre-strain accelerates the precipitation sequence of the Al-Zn-Mg-Cu alloy, the lower strength of pre-strained plates was attributed to the coarsened and low density of MPts. When the plates were subjected to 6% pre-strain, numerous incoherent η phase can be observed within in the grains.
2. Compared with the un-strained samples, pre-strain can significantly improve the comprehensive corrosion resistance of the Al-Zn-Mg-Cu alloy owing to the discontinuous and larger inter-space GBPs, wider PFZ and residual dislocations.
3. Among all the pre-strained samples, the 2% pre-strained sample exhibits the best comprehensive performance with optimal corrosion resistance and minimal strength loss; further increasing the pre-strain level, the high-density

dislocation and coarsened precipitates within matrix and at grain boundaries accelerated the enrichment of hydrogen at the tip of corrosion crack, resulting in lower corrosion resistance compared with the samples with 2% pre-strain.

Acknowledgments

The research is under the support of the Department of Material Science and Engineering, Central South University, Changsha, China; and the Major Special Projects of Hunan Province (No. 2023GK1080).

Author Contributions

Mengjun Long involved in methodology, investigation, and writing—original draft. Feng Jiang involved in validation and writing—review and editing. Feifei Wu: involved in methodology. Mingjin Wu involved in investigation and software. Yuanming Su involved in formal analysis.

Competing interests

The authors declare that they have no known competing financial interests or personal relationships that could have appeared to influence the work reported in this paper.

References

1. J.C. Williams and E.A. Starke, Progress in Structural Materials for Aerospace Systems, *Acta Mater.*, 2003, **51**, p 5775–5799.
2. P.A. Rometsch, Y. Zhang, and S. Knight, Heat Treatment of 7xxx Series Aluminum Alloys-Some Recent Developments, *Trans. Nonferrous Metal. Soc.*, 2014, **24**, p 2003–2017.
3. M.A. Krishnan and V.S. Raja, Development of High Strength AA 7010 Aluminum Alloy Resistant to Environmentally Assisted Cracking, *Corros. Sci.*, 2016, **109**, p 94–100.
4. A. Heinz, A. Haszler, C. Keidel, S. Moldenhauer, R. Benedictus, and W.S. Miller, Recent Development in Aluminium Alloys for Aerospace Applications, *Mater. Sci. Eng. A*, 2000, **280**, p 102–107.
5. J.H. Zhao, Y.L. Deng, J.G. Tang, and J. Zhang, Effect of Gradient Grain Structures on Corrosion Resistance of Extruded Al-Zn-Mg-Cu Alloy, *J. Alloys Compd.*, 2020, **832**, 154911
6. T. Marlaud, A. Deschamps, F. Bley, W. Lefebvre, and B. Baroux, Influence of Alloy and Heat Treatment on Precipitate Composition in Al-Zn-Mg-Cu Alloys, *Acta Mater.*, 2010, **58**, p 248–260.
7. J. Buha, R.N. Lumley, and A.G. Crosky, Secondary Ageing in an Aluminum Alloy 7050, *Mater. Sci. Eng. A*, 2008, **492**, p 1–10.
8. A.F. Oliveira Jr., M.C. de Barros, K.R. Cardoso, and D.N. Travessa, The Effect of RRA on the Strength and SCC Resistance on AA7050 and AA7150 Aluminium Alloys, *Mater. Sci. Eng. A*, 2004, **379**, p 321–326.
9. T.S. Zhao, J. Zhou, J.F. Zhou, D.X. Wu, and Y. Xiong, Influence of Pre-stretching and Aging Processes on Comprehensive Performance of Aluminum Alloy, *Mater. Manuf. Process.*, 2018, **33**, p 1641–1647.
10. T. Ogura, T. Otani, A. Hirose, and T. Sato, Improvement of Strength and Ductility of an Al-Zn-Mg Alloy by Controlling Grain Size and Precipitate Microstructure with Mn and Ag Addition, *Mater. Sci. Eng. A*, 2013, **580**, p 288–293.
11. P. Xia, Z.Y. Liu, S. Bai, L.Q. Lu, and L.F. Gao, Enhanced Fatigue Crack Propagation Resistance in a Super High Strength Al-Zn-Mg-Cu Alloy by Modifying RRA Treatment, *Mater Charact*, 2016, **118**, p 438–445.
12. D.L. Yuan, K.H. Chen, S.Y. Chen, L.P. Huang, G. Chen, and S.J. Chen, Effect of Pre-strain and Quench Rate on Stress Corrosion Cracking Resistance of a Low-Cu Containing Al-Zn-Mg-Cu Alloy, *Mater. Sci. Eng. A*, 2022, **833**, 142374
13. M.B. Prime and M.R. Hill, Residual Stress, Stress Relief, and Inhomogeneity in Aluminum Plate, *Scr. Mater.*, 2002, **46**, p 77–82.
14. J.J. Hoyt, On the Coarsening of Precipitates Located on Grain Boundaries and Dislocations, *Acta Metall. Mater.*, 1991, **39**, p 2091–2098.
15. K. Ma, T. Hu, H. Yang, T. Topping, A. Yousefiani, E.J. Lavernia, and J.M. Schoenung, Coupling of Dislocations and Precipitates: Impact on the mechAnical Behavior of Ultrafine Grained Al-Zn-Mg Alloys, *Acta Mater.*, 2016, **103**, p 153–164.
16. M. Legros, G. Dehm, E. Arzt, and T. John Balket, Observation of Giant Diffusivity Along Dislocation Cores, *Science*, 2008, **319**, p 1646–1649.
17. X.D. Wang, Q.L. Pan, W.Y. Wang, Z.Q. Huang, J. Chen, B.Q. Pan, and X. Liu, Effect of Pre-strain and Aging Treatment on the Mechanical Property and Corrosion Resistance of the Spray Formed Ultra-high Strength Al-Zn-Mg-Cu Alloy, *Mater Charact*, 2022, **194**, 112381
18. N.M. Han, X.M. Zhang, S.D. Liu, B. Ke, and X. Xin, Effects of Pre-stretching and Ageing on the Strength and Fracture Toughness of Aluminum Alloy 7050, *Mater. Sci. Eng. A*, 2011, **528**, p 3714–3721.
19. C.R. Shastry and M. Levy, Effect of Tensile Deformation and Heat Treatment on the Stress Corrosion Susceptibility of an Al-Zn-Mg-Cu Alloy, *Met. Technol.*, 1974, **1**, p 547–550.
20. L.H. Lin, Z.Y. Liu, W.W. Zhang, and H.J. Peng, Effects of Pre-strain on the Surface Residual Stress and Corrosion Behavior of an Al-Zn-Mg-Cu Alloy plate, *Mater Charact*, 2020, **160**, 110129
21. D. Wang and Z.Y. Ma, Effect of Pre-strain on Microstructure and Stress Corrosion Cracking of Over-Aged 7050 Aluminum Alloy, *J. Alloys Compd.*, 2009, **469**, p 445–450.
22. Y. Zou, X.D. Wu, S.B. Tang, Y.C. Wang, K. Zhao, and L.F. Cao, The Effect of Pre-ageing/Stretching on the Ageing-Hardening Behavior of Al-Zn-Mg-Cu Alloys Correlated with Zn/Mg Ratio, *Mater. Sci. Eng. A*, 2022, **830**, 142331
23. K.Z. He, Q. Li, S.D. Liu, X.M. Zhang, and K.Z. Zhou, Influence of Pre-stretching on Quench Sensitive Effect of High-Strength Al-Zn-Mg-Cu-Zr Alloy Sheet, *J. Cent. South Univ.*, 2021, **28**, p 2660–2669.
24. X.W. Ren, Y.X. Zhang, X. Zhao, Z.M. Zhang, Q. Wang, S.Q. Wang, Y.Y. He, and H.L. Liu, Influence of Overlap Precipitate on the Strength–Ductility Synergy of the Al-10.0Zn-3.0Mg-2.5Cu Alloy with a New Aging Strategy, *J. Mater. Res. Technol.*, 2023, **23**, p 2730–2739.
25. Z.Y. Zhong, H.-G. Brokmeier, W.M. Gan, E. Maawad, B. Schwebke, and N. Schell, Dislocation Density Evolution of AA 7020–T6 Investigated by In-Situ Synchrotron Diffraction Under Tensile Load, *Mater Charact*, 2015, **108**, p 124–131.
26. J.Y. Jiang, F. Jiang, H.F. Huang, M.H. Zhang, Z.Q. Tang, and M.M. Tong, Hot Deformation Analysis and Microstructure Evolution of Al-Mg-Mn-Sc-Zr Alloy by Isothermal Compression, *J. Alloys Compd.*, 2021, **858**, 157655
27. M.M. Tong, F. Jiang, H.L. Wang, J.Y. Jiang, P.C. Ye, and X.D. Xu, The Evolution of Mechanical Properties and Microstructures of Al-Mg-Mn-Sc-Zr Alloy During Dynamic Stretching Deformation, *J. Alloys Compd.*, 2021, **889**, 161753
28. K.B. Hyde, A.F. Norman, and P.B. Prangnell, The Effect of Cooling Rate on the Morphology of Primary Al_3Sc Intermetallic Particles in Al-Sc Alloys, *Acta Mater.*, 2001, **49**, p 1327–1337.
29. W.Y. Wang, Q.L. Pan, X.D. Wang, J. Ye, Z.Q. Huang, S.Q. Xiang, and B. Liu, Effect of Laser Shock Peening on Corrosion Behaviors of Ultra-high Strength Al-Zn-Mg-Cu Alloys Prepared by Spray Forming and Ingot Metallurgy, *Corros. Sci.*, 2022, **205**, 110458
30. Z.Q. Tang, F. Jiang, P. Xu, J.Y. Jiang, J.J. Zeng, L.Y. Lu, and M.M. Tong, Investigation on Microstructure, Mechanical Properties and Corrosion Behavior of VPPA Welded Al-Mg-Mn-Sc-Zr Alloy, *Mater. Today Commun.*, 2020, **25**, 101480
31. S.P. Knight, N. Birbilis, B.C. Muddle, A.R. Trueman, and S.P. Lynch, Correlations Between Intergranular Stress Corrosion Cracking, Grain-Boundary Microchemistry, and Grain-Boundary Electrochemistry for Al-Zn-Mg-Cu Alloys, *Corros. Sci.*, 2010, **52**, p 4073–4080.
32. S. Li, H. Dong, P. Li, and S. Chen, Effect of Repetitious Non-isothermal Heat Treatment on Corrosion Behavior of Al-Zn-Mg Alloy, *Corros. Sci.*, 2021, **180**, 109174

33. S.Y. Zhang, Y.X. Wu, and H. Gong, A Modeling of Residual Stress in Stretched Aluminum Alloy Plate, *J. Mater. Process. Technol.*, 2012, **212**, p 2463–2473.
34. J. Huang, M. Meyer, and V. Pontikis, Is Pipe Diffusion in Metals Vacancy Controlled: A Molecular Dynamics Study of an Edge Dislocation in Copper, *Phys. Rev. Lett.*, 1989, **63**, p 628–631.
35. L. Lin, Z. Liu, X. Han, and W. Liu, Effect of Overaging on Fatigue Crack Propagation and Stress Corrosion Cracking Behaviors of an Al-Zn-Mg-Cu Alloy Thick Plate, *J. Mater. Eng. Perform.*, 2018, **27**, p 3824–3830.
36. J.C. Li and J. Dang, A summary of Corrosion Properties of Al-Rich Solid Solution and Secondary Phase Particles in Al Alloys, *Metals.*, 2022, **7**, p 84–102.
37. J.F. Li, Z.Q. Zheng, S.C. Li, W.J. Chen, W.D. Ren, and X.S. Zhao, Simulation Study on Function Mechanism of Some Precipitates in Localized Corrosion of Al Alloys, *Corros. Sci.*, 2007, **49**, p 2436–2449.
38. E. Diler, B. Lescop, S. Rioual, G. Nguyen Vien, D. Thierry, and B. Rouvellou, Initial Formation of Corrosion Products on Pure Zinc and $MgZn_2$ Exanimated by XPS, *Corros. Sci.*, 2014, **79**, p 83–88.
39. M.-S. Oh, S.-H. Kim, J.-S. Kim, J.-W. Lee, J.-H. Shon, and Y.-S. Jin, Surface and Cut-Edge Corrosion Behavior of Zn-Mg-Al Alloy-Coated Steel Sheets as a Function of the Alloy Coating Microstructure, *Met. Mater. Int.*, 2015, **22**, p 26–33.
40. J.F. Chen, X.F. Zhang, L.C. Zou, Y. Yu, and Q. Li, Effect of Precipitate State on the Stress Corrosion Behavior of 7050 Aluminum Alloy, *Mater Charact*, 2016, **114**, p 1–8.
41. G.M. Scamans, Discontinuous Propagation of Stress Corrosion Cracks in Al-Zn-Mg Alloys, *Scr. Metall.*, 1979, **13**, p 245–250.
42. H. Kamoutsi, G.N. Haidemenopoulos, V. Bontozoglou, P.V. Petroyiannis, and S.G. Pantelakis, Effect of Prior Deformation and Heat Treatment on the Corrosion-Induced Hydrogen Trapping in Aluminium Alloy 2024, *Corros. Sci.*, 2014, **80**, p 139–142.
43. L. Oger, B. Malard, G. Odmer, L. Peguet, and C. Blanc, Influence of Dislocations on Hydrogen Diffusion and Trapping in an Al-Zn-MgCu Aluminium Alloy, *Mater. Des.*, 2019, **180**, 107901

Publisher's Note Springer Nature remains neutral with regard to jurisdictional claims in published maps and institutional affiliations.

Springer Nature or its licensor (e.g. a society or other partner) holds exclusive rights to this article under a publishing agreement with the author(s) or other rightsholder(s); author self-archiving of the accepted manuscript version of this article is solely governed by the terms of such publishing agreement and applicable law.